The Astrophysical Journal Letters, 863:L7 (6pp), 2018 August 10 https://doi.org/10.3847/2041-8213/aad62e

BST1047+1156: An Extremely Diffuse and Gas-rich Object in the Leo I Group

J. Christopher Mihos[1], Christopher T. Carr[1], Aaron E. Watkins[2], Tom Oosterloo[3,4], and Paul Harding[1]
[1] Department of Astronomy, Case Western Reserve University, USA
[2] Astronomy Research Unit, University of Oulu, Finland
[3] Netherlands Institute for Radio Astronomy (ASTRON), The Netherlands
[4] Kapteyn Astronomical Institute, University of Groningen, The Netherlands
Received 2018 June 27; revised 2018 July 25; accepted 2018 July 25; published 2018 August 6

Abstract

We report the detection of diffuse starlight in an extragalactic H I cloud in the nearby Leo I galaxy group. We detect the source, BST1047+1156, in both broadband optical and the *Galaxy Evolution Explorer* (*GALEX*) ultraviolet (UV) light. Spanning ∼2 kpc in radius, it has a peak surface brightness of $\mu_B = 28.8$ mag arcsec^{-2}, making it the lowest surface brightness object ever detected via integrated light. Although the object is extremely gas rich, with a gas fraction of $f_g = 0.99$, its peak H I column density is well below levels where star formation is typically observed in galaxies. Nonetheless, BST1047+1156 shows evidence for young stellar populations: along with the detected UV emission, the object is extremely blue, with $B - V = 0.14 \pm 0.09$. The object has two tidal tails and is found embedded within diffuse gas connecting the spiral galaxy M96 to the group's extended H I Leo Ring. The nature of BST1047+1156 is unclear. It could be a disrupting tidal dwarf, recently spawned from star formation triggered in the Leo I group's tidal debris. Alternatively, the object may have been a pre-existing galaxy—the most extreme example of a gas-rich field low surface brightness galaxy known to date—which had a recent burst of star formation triggered by encounters in the group environment.

Key words: galaxies: evolution – galaxies: groups: individual (Leo I) – galaxies: interactions – galaxies: irregular – galaxies: structure

1. Introduction

As optical imaging studies probe to deeper limits, the discovery of galaxies at ever-lower low surface brightnesses continues to challenge models of galaxy formation and evolution. Much attention has been paid to the extremely diffuse galaxies found in cluster environments (e.g., Sandage & Binggeli 1984; Impey et al. 1988; Caldwell 2006; Mihos et al. 2015; van Dokkum et al. 2015), but in dense clusters it is difficult to disentangle questions of galaxy formation from those of subsequent dynamical evolution due to the various heating and stripping processes at work in dense environments. In contrast, the gas-rich low surface brightness (LSB) galaxies found in low-density environments (e.g., McGaugh & Bothun 1994; McGaugh & de Blok 1997; Cannon et al. 2015, Leisman et al. 2017) should have a less complicated evolutionary path, and may better probe mechanisms of galaxy formation.

The high gas fractions found in field LSB galaxies (with $f_g \equiv M_{\rm gas}/(M_{\rm gas} + M_*)$ as high as 0.98, Janowiecki et al. 2015; Ball et al. 2018) argue that these systems are largely unevolved. Under canonical models for galaxy formation, such galaxies may have formed relatively late in the universe's history from the collapse of high angular momentum material (e.g., Dalcanton et al. 1997; Mo et al. 1998; Amorisco & Loeb 2016). Alternatively, some fraction of these systems may have instead condensed within gas-rich tidal debris stripped from galaxies during close encounters (e.g., Duc et al. 2000; Weilbacher et al. 2000; Bournaud et al. 2004; Lelli et al. 2015). If these "tidal dwarf" galaxies survive subsequent dynamical destruction, they would represent a population of low-mass, gas-rich galaxies distinct from classical dwarfs formed by the collapse of material onto dark matter halos.

Regardless of their formation history, such objects also probe star formation processes in low-density environments. Their low gas densities are often at or below that required for widespread star formation (van der Hulst et al. 1993; van Zee et al. 1997; Wyder et al. 2009), resulting in sputtering and inefficient star formation histories (Schombert et al. 2001; Schombert & McGaugh 2014, 2015). These effects may limit their ability to form a substantial stellar disk, suggesting that absent subsequent dynamical evolution there may well be a fundamental "floor" to galaxy surface brightness set by the ability to form star at low surface densities. Probing the lower limits to galaxy surface brightness is thus critically important for models of both galaxy formation and star formation.

Here we report the detection of diffuse starlight in an extragalactic cloud in the nearby Leo I galaxy group ($d = 11$ Mpc; Graham et al. 1997; Jang & Lee 2017). We detect the system, named BST1047+1156 (hereafter BST1047), in optical broadband and *Galaxy Evolution Explorer* (*GALEX*) ultraviolet (UV) light and confirm its kinematic association with tidal gas in the Leo I group. With an extremely low peak surface brightness of $\mu_B \approx 28.8$ mag arcsec^{-2}, BST1047 is the most diffuse object yet detected via integrated starlight. The system may be the evolved counterpart of star-forming regions in the group's extended H I ring, a tidal dwarf possibly undergoing disruption. Alternatively, it may be a pre-existing LSB galaxy tidally perturbed by encounters within the group environment. In this Letter, we compare BST1047 to other types of LSB galaxies, and consider various evolutionary scenarios to describe this extreme system.

2. Optical Detection and H I Mapping

The optical imaging used here was originally taken as part of a deep search for intragroup light in the Leo I group, and is described in detail in Watkins et al. (2014, hereafter W+14). We imaged Leo I over two seasons with Case Western Reserve University's (CWRU's) Burrell Schmidt telescope, using a modified Johnson B filter (spring 2012) and Washington M

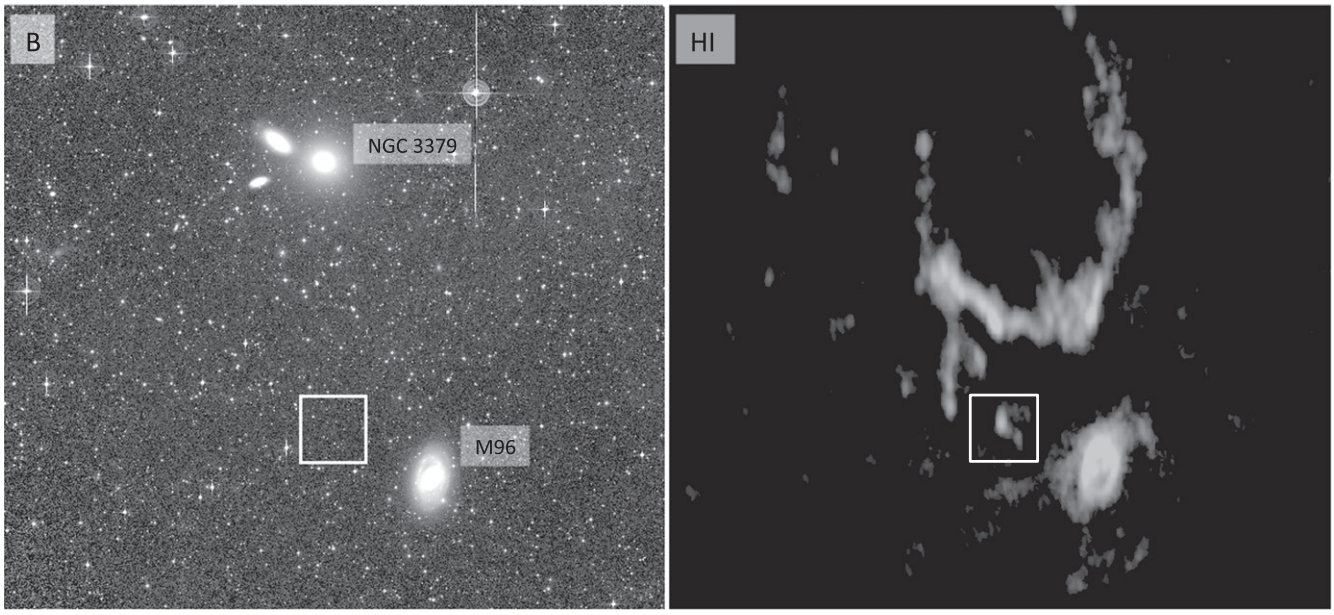

Figure 1. Wide-field ($1.^{\circ}5 \times 1.^{\circ}6$) B-band image (left) and 21 cm H I map (right) of the Leo I group (from Watkins et al. 2014 and Oosterloo et al. 2010, respectively). BST1047 is located at the center of the white box, whose $9.'5 \times 9.'5$ size matches the field of view of Figure 2.

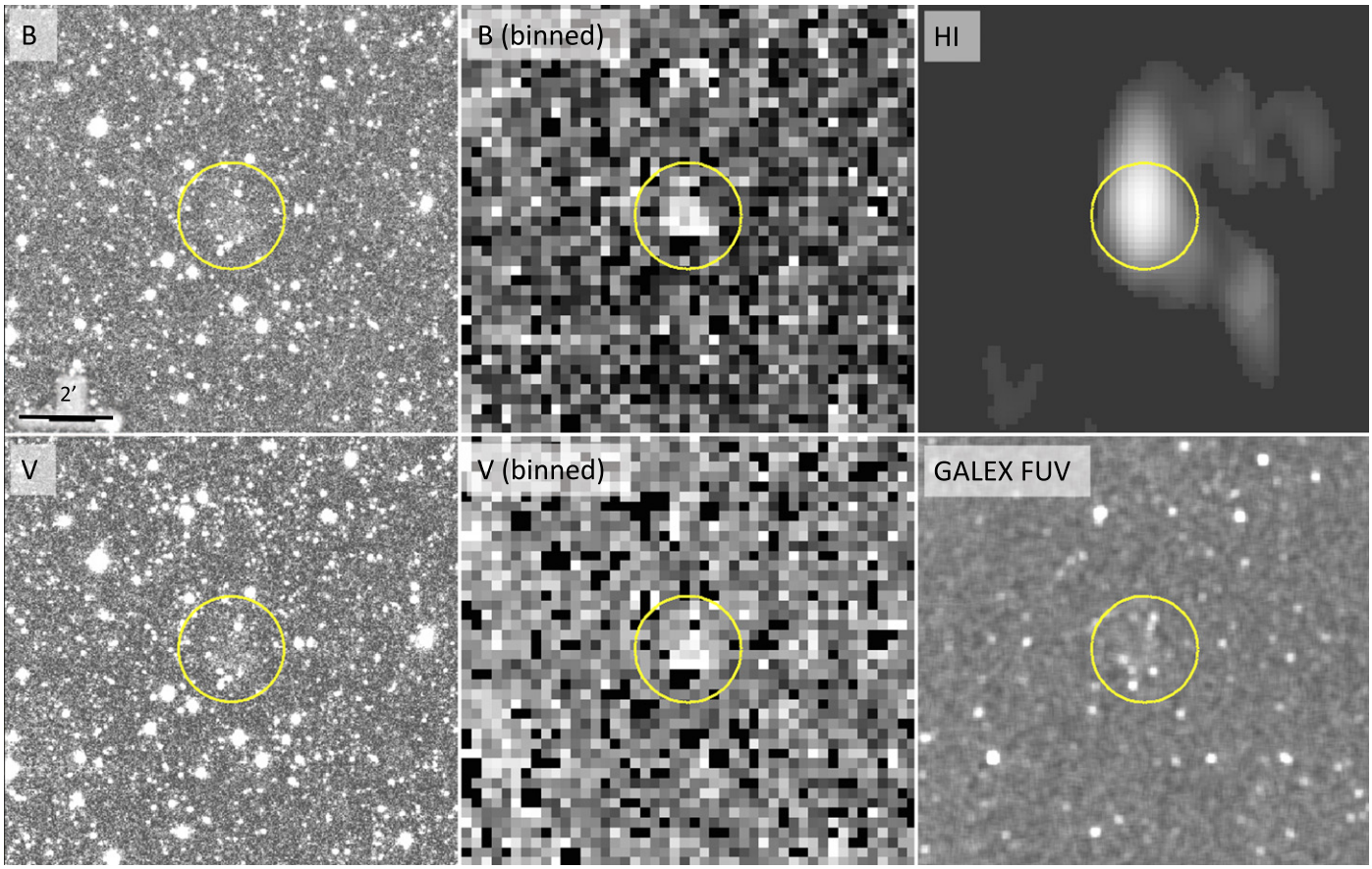

Figure 2. Imaging of BST1047 at multiple wavelengths. Optical imaging is shown in the left panels; the center panels show the optical images after masking compact sources and median binning to $13'' \times 13''$ resolution. The upper-right panel shows the H I map. The lower-right panel shows the *GALEX* far-UV (FUV) image, boxcar smoothed 3×3 ($4.''5 \times 4.''5$) to show faint detail. The yellow circle has a radius of $70''$, *twice* the size of the R_{30} isophote.

filter (spring 2013). We used a dither-and-stack technique (W+14) with a total observing time of 13.7 and 10.25 hr in B and M, respectively. The resulting mosaics (Figure 1) covered $\sim$2.4 $\times$ 2.4 degree^2 at 1.45 arcsec pixel^{-1} and have a liming depth of $\mu_B = 30.0$ and $\mu_V = 29.5$ mag arcsec^{-2} after transformation to Johnson Vega magnitudes.

While W+14 discussed the properties of diffuse light on large scales in the Leo I group, BST1047 was only discovered

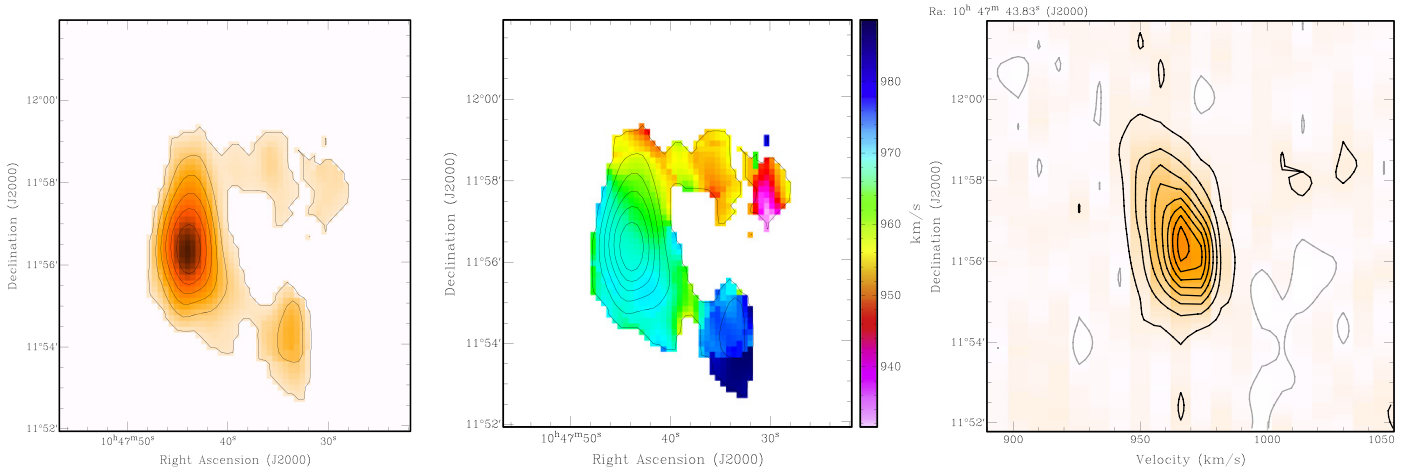

Figure 3. Left: H I column density, with contours shown at 1.1, 3.3, 5.5, 7.7, 9.9, and 11.1 $\times$ 10^{19} cm^{-2}. Center: 2D velocity field. Right: N/S position–velocity cut through the object.

when one of us (C.T.C.) undertook a more detailed search for LSB objects on smaller scales. We detect BST1047 in both optical bands, projected 15.′7 (50 kpc) ENE of the spiral galaxy M96. While the object is extremely faint, with a peak surface brightness of $\mu_B = 28.8$, the fact that it appears in *independent* image stacks taken in different seasons and comprising many overlapping, dithered images rules out the possibility of scattered light or instrumental artifacts. By masking compact sources in the image and comparing the flux in the object to that measured in 30″ apertures scattered randomly around the source, we find the object is detected at the 5.4σ and 4.3σ level in B and V, respectively. Figure 2 shows a close-up view of BST1047 at different wavelengths, where the optical images are shown both at full resolution and after being masked and binned to enhance the diffuse light.

After the optical discovery, comparison of the imaging to H I mapping of the Leo I group (Schneider 1985; Schneider et al. 1986, 1989, Haan et al. 2009; Oosterloo et al. 2010) revealed an H I source that is spatially coincident with the optical detection. Although the H I detection precedes our deep optical study, we emphasize that our detection of BST1047 was a purely optical one, with no prior knowledge by C.T.C. of the H I imaging data. To our knowledge, this makes BST1047 the lowest surface brightness object ever discovered via integrated light.

Figure 1 shows the Westerbork H I map of the Leo I group obtained after reprocessing the observations of Oosterloo et al. (2010). The spatial resolution is 105.″0 $\times$ 39.″2 (PA = 0°), and the noise level is 0.70 mJy beam^{-1} for a velocity resolution of 8.0 km s^{-1}. The H I data is shown in detail in Figure 3. The H I line is only marginally resolved in velocity, with an observed (Gaussian) line width of $\sigma = 9.0 \pm 1.0$ km s^{-1}. While the object's N–S elongation is partly due to the noncircular beam of the telescope, a small velocity gradient across the main body indicates that the source is slightly resolved spatially as well. On larger scales, the object is found near the gas seen extending southward from the Leo Ring in Figure 1, and is in fact embedded in a stream of gas connecting the Ring to M96 at even lower column densities (Schneider 1985; Schneider et al. 1989). BST1047 also shows two diffuse H I tails stretching toward M96 to the west, suggestive of tidal or ram pressure stripping. The object's systemic velocity (970 km s^{-1}) is similar to that of M96 (897 km s^{-1}) and NGC 3379 (911 km s^{-1}), and unambiguously places it within the Leo I group.

3. Source Properties

BST1047's extremely diffuse nature makes quantitative photometry challenging. The object is roughly 35″ in radius before dropping below the limiting surface brightness of $\mu_B = 30.0$ mag arcsec^{-2}, and within this radius are a number of compact sources. These sources span a range of $B - V$ colors similar to star-forming knots observed in other LSB galaxies (Schombert et al. 2013), making it possible that some of these sources could be intrinsic to the object itself. However, these sources are spatially consistent with being background contaminants, as they are not centrally concentrated in the system but are found largely in the outskirts at $r > 25''$. Here we take the conservative approach of masking these sources and measuring the photometric properties of the diffuse light only. Furthermore, given BST1047's irregular surface brightness profile and low signal-to-noise ratio (S/N), the object is not amenable to traditional profile fitting. Instead, we give nonparametric estimates of the limiting $\mu_B = 30$ isophotal size (R_{30}), the effective radius (R_e) containing half of the light encompassed within R_{30}, the mean surface brightness within R_e ($\langle\mu_B\rangle_e$), and the total integrated magnitudes and colors. These values are reported in Table 1, corrected for foreground reddening using $A_B = 0.09$, $E(B - V) = 0.02$ (Schlafly & Finkbeiner 2011).

Figure 4 shows BST1047's surface brightness profile, with errorbars reflecting both the ∼5″ positional uncertainty in the optical center as well as background uncertainties (measured from 30″ sky apertures scattered randomly in the surrounding field). Not only is the object diffuse, with an average surface brightness of $\langle\mu_B\rangle_e = 28.9$ mag arcsec^{-2}, it has a flat luminosity profile with no evidence for central concentration. Summing the diffuse light within R_{30} yields a total magnitude of $m_B = 20.02^{+0.14}_{-0.13}$, and an extremely blue color of $(B - V) = 0.14^{+0.09}_{-0.09}$.

Given the object's very blue color, we also searched for it in *GALEX* UV imaging (Figure 2). In both FUV and near-UV (NUV) we recover many of the compact sources, along with weak, diffuse UV flux detected at the 3.4σ (FUV) and 3.7σ (NUV) levels. This diffuse UV light has a FUV − NUV color

Table 1
BST1047+1156

Optical Center (J2000)	(10:47:43.8, +11:56:01)
R_{30}	35″ (1.85 kpc)
R_e	22″ (1.2 kpc)
$\langle\mu_B\rangle_e$	28.9 mag arcsec^{-2}
m_B, m_V (Vega)	$20.02^{+0.14}_{-0.13}$, $19.86^{+0.22}_{-0.16}$
$(B-V)$	$0.14^{+0.09}_{-0.09}$
M_B	−10.2
L_B	$1.85 \times 10^6\ L_\odot$
$m_{\rm FUV}$, $m_{\rm NUV}$ (AB)	$21.66^{+0.25}_{-0.17}$, $21.19^{+0.20}_{-0.16}$
(FUV − NUV)	$0.47^{+0.29}_{-0.26}$
H I peak (J2000)	(10:47:43.8, +11:56:18)
H I flux	1.59 Jy km s^{-1}
H I mass	$4.5 \times 10^7\ M_\odot$
$\Sigma_{\rm H\ I,peak}$	1.4×10^{20} cm^{-2}
v_{sys}	970 km s^{-1}

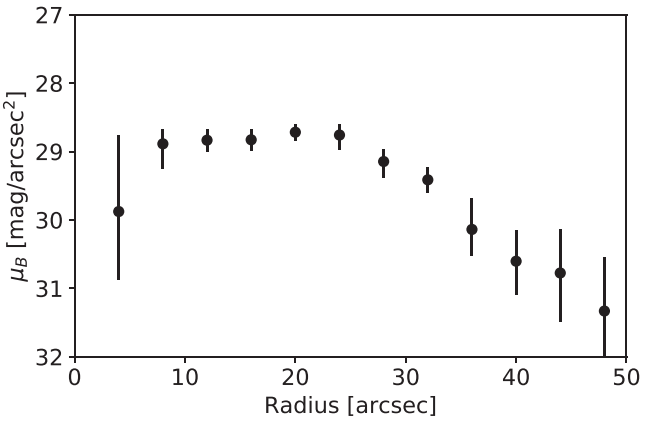

Figure 4. B-band surface brightness profile of BST1047.

of $0.47^{+0.29}_{-0.26}$, after correction for foreground reddening (Thilker et al. 2009). The detected FUV emission suggests that the system has experienced recent star formation over the past few hundred Myr (i.e., the FUV-emitting lifetime of young stellar populations; Kennicutt & Evans 2012).

BST1047 has a total H I flux of 1.59 Jy km s^{-1}, giving an H I mass of $M_{\rm H\,I} = 4.5 \times 10^7\ M_\odot$, or a total gas mass (correcting for helium) of $M_{\rm gas} = 1.33 \times M_{\rm H\,I} = 6 \times 10^7\ M_\odot$. Adopting a stellar mass-to-light ratio of $M_*/L_B = 0.2$, appropriate for stellar populations with the colors measured here (Bell & de Jong 2001), yields a stellar mass of $M_* = 3.7 \times 10^5\ M_\odot$ and gas fraction $f_g = 0.99$, rivaling the most extreme measured for any galaxy (e.g., Janowiecki et al. 2015). However, the gas is quite diffuse, with peak H I column density 1.4×10^{20} cm^{-2}, well below levels at which star formation typically occurs (e.g., Bigiel et al. 2008, 2010; Krumholz et al. 2009; Clark & Glover 2014). This result is seemingly at odds with the blue optical colors and FUV emission, both indicators of recent star formation. Given the relatively large beam size of the Westerbork data, pockets of higher density gas could exist on smaller scales to drive star formation, although no Hα emission was detected in deep narrowband imaging of the group by Donahue et al. (1995).

Indeed, the properties of BST1047 are so extreme that they may call into question the likelihood that we are seeing bona-fide starlight at all. At these faint surface brightnesses, deep imaging surveys are plagued by contamination due to scattered light from Milky Way dust (the Galactic cirrus; see, e.g., Mihos et al. 2017), but this is not a concern here. The object is not detected in infrared emission (a common tracer of Galactic dust) in either the *Wide-field Infrared Survey Explorer* (*WISE*) 12 μm or IRIS 100 μm maps (Miville-Deschênes & Lagache 2005; Meisner & Finkbeiner 2004, respectively), and the measured H I velocity of the system lies well outside the range of Milky Way high-velocity clouds (Wakker & van Woerden 1997). However, a second possibility is scattering from dust in the object at the Leo I distance. A simple calculation shows this to be unlikely. The closest source of optical photons is M96, projected 50 kpc to the west. If we take the flux impingent on BST1047 from M96 and use the dust scattering model of Draine (2003) to scatter that light along our line of sight, the *maximum* observed surface brightness achieved is $\mu_B \sim 31$ mag arcsec^{-2}, significantly fainter than observed. Because dust preferentially forward-scatters light, this maximum surface brightness is achieved only in the specific situation where BST1047 lies 50 kpc in front of M96 (as well as 50 kpc in transverse projection); other geometries predict even lower surface brightnesses due either to the scattering phase function or a larger separation from M96 reducing the impingent stellar light on BST1047. Furthermore, the Draine model adopts a Milky Way dust-to-gas ratio and likely overestimates the dust content of BST1047 by a significant amount. As a result, scattering of M96 starlight from dust within BST1047 is unlikely to explain the diffuse light that we observe.

4. Discussion

What is BST1047? One natural comparison is to the star-forming knots embedded in the Leo Ring to the north (Thilker et al. 2009; Michel-Dansac et al. 2010; W+14). Compared to these complexes, BST1047 is similar in size and H I mass, but fainter in FUV light and somewhat redder in UV color ($(\rm FUV-NUV)_{knots} = -0.3$ to $+0.05$). This suggests that the system may be an older, more evolved version of the star-forming complexes seen in the Leo Ring, observed after star formation has largely died out. Using the FUV star formation rate (SFR) estimator of Hunter et al. (2010) gives a total SFR for BST1047 of $\sim 1.4 \times 10^{-4}\ M_\odot$ yr^{-1} (lower by a factor of 4–5 compared to the star-forming knots in the Ring). At this rate, the time to build the observed stellar mass is ∼3 Gyr, but continuous star formation would produce stellar populations that are too red to match the observed optical color. A rapidly declining SFR is also indicated by the lack of detected Hα in the imaging of Donahue et al. (1995)—adopting the Hα-SFR calibration of Murphy et al. (2011) gives an upper limit to the *current* SFR of $\sim 5 \times 10^{-5}\ M_\odot$ yr^{-1}, down by nearly a factor of three compared to that inferred from the FUV light, which traces the SFR over longer 100–200 Myr timescales. Hence, the FUV emission and blue colors seen in BST1047 could be tracing a *post-burst* stellar population formed by recent star formation. A comparison of the optical and UV colors to stellar population synthesis models (Leitherer et al. 1999; Bruzual & Charlot 2003) shows consistency with population ages of 200–600 Myr.

The similarity in H I mass and size between Leo Ring clumps and known dwarf galaxies has led several authors to suggest the Ring clumps may be tidal dwarf galaxies in formation (e.g., Schneider et al. 1986; Thilker et al. 2009). BST1047 may be a similar and somewhat older object transitioning to a quiescent evolutionary stage. In this scenario,

the BST1047's spatial and kinematic association with the diffuse gas connecting the Leo Ring to M96 suggest that it may have formed during an interaction between M96 and the Ring. The stellar population age inferred above sets the timescale for such an event at ∼200–600 Myr ago, somewhat shorter than the ∼1 Gyr old interaction age hypothesized by Michel-Dansac et al. (2010) in their model of the formation of the Leo Ring. If that model is correct, the interaction that gave rise to BST1047 may be secondary to that which formed the Ring itself.

Tidal dwarfs are expected to be free of dark matter, having condensed due to the compression of tidal gas. If the kinematics of BST1047 trace the gravitational potential, we can infer its dynamical mass using the estimator of Hoffman et al. (1999):

$$M_{\rm dyn} = 2.325 \times 10^5 \left(\frac{V_{\rm rot}^2 + 3\sigma^2}{\rm km^2\ s^{-2}}\right)\left(\frac{R}{\rm kpc}\right) M_\odot.$$

For BST1047, several factors complicate this analysis. First, it is unclear if the observed velocity gradient reflects tidal shear or true rotation, and, furthermore, if the system is rotating we have little information on its inclination. Also, the H I line width is only slightly resolved over instrumental, making a reliable measurement of the intrinsic velocity dispersion difficult. Nonetheless, if we presume that the gradient is rotational, we can estimate $V_{\rm rot}$ as half the N–S velocity difference measured at 20% peak H I intensity (the second positive contour in Figure 3(c)), which gives $V_{\rm rot} = 8\ {\rm km\ s^{-1}}$. Taking the quadrature difference between the observed Gaussian line width and the instrumental dispersion yields an intrinsic velocity dispersion of $\sigma = 4\ {\rm km\ s^{-1}}$. Using these values along with the $R_{30} = 1.85$ kpc isophotal radius yields $M_{\rm dyn} = 4.8 \times 10^7\ M_\odot$, comparable to the observed baryonic mass ($6 \times 10^7\ M_\odot$). Although consistent with the tidal dwarf scenario in which baryons provide all the dynamical mass, our mass estimate is very uncertain; if the system is observed largely face-on, any inclination correction would increase $M_{\rm dyn}$, while a lack of rotation would drop $M_{\rm dyn}$ to only one-third of the baryonic mass.

The survival of a tidal dwarf depends on a complicated balance between its binding mass (set only by the baryons), energy injection from massive stars, and dynamical stripping by the local environment. BST1047's H I tidal tails indicate that the object is being stripped as it moves through the Leo I group. This stripping, coupled possibly with energy injection from the initial starburst, could have driven gas densities down to the current levels that inhibit continuing star formation. The initial compression of gas that formed BST1047 may now be "rebounding," and the stars—following the gravitational potential dominated by the gas—would disperse as well, leading to the flat surface brightness profile seen in Figure 4. Thus, the object we see today might only be transitory—recently formed, but in the process of disruption in the group environment.

In this scenario, then, BST1047 might be a *failed* (or failing) tidal dwarf, with little or no ongoing star formation and insufficient binding mass to ensure its survival. While prospective tidal dwarfs in some other systems appear to have sufficient mass to survive subsequent destruction (e.g., Lelli et al. 2015), BST1047 suggests that not all systems might be so lucky. Gas-rich interactions could lead to the formation and expulsion of fragile dwarfs from their host galaxies, after which they are destroyed and dispersed into intergalactic space, adding to the population of intragroup or intracluster stars found in many high-density environments. In the Leo I group we may be witnessing the full evolutionary path of these objects, from formation (the star-forming knots) through disruption (BST1047) and ending with dispersal in the form of the extended and faint "orphan" stellar streams observed in group (see Figure 2 of W+14).

However, an alternative explanation might be that rather than being a tidally spawned object, BST1047 is instead a pre-existing, extremely diffuse LSB galaxy, perhaps a satellite companion of M96, that has been caught in a tidal interaction within the group. If the object is an M96 satellite, another analog might be the diffuse star-forming satellites in and around the Local Group, such as Leo T (Irwin et al. 2007; Ryan-Weber et al. 2008) and Leo P (McQuinn et al. 2013, 2015). Compared to these systems, BST1047 is significantly larger ($r_e \sim 1$ kpc, compared to 0.1–0.2 kpc for Leo T and Leo P) and more luminous (by 1–2 mag), with a much higher gas mass (by two orders of magnitude). However, the key factor that differentiates BST1047 is not just size but density. Both Leo P and Leo T have central surface brightnesses of $\mu_V \approx 24.5\ {\rm mag\ arcsec^{-2}}$, 50 times higher in luminosity density than BST1047. And while Leo P and Leo T are significantly lower in gas mass, their compact nature means that their H I column densities are actually several times *higher* than those found in BST1047. In BST1047, the low gas density likely means that the object has been even less efficient than Leo P or Leo T at forming stars, and may explain its extremely high gas fraction ($f_g = 0.99$, compared to $f_g = 0.8$ and 0.6 for Leo T and Leo P, respectively; Ryan-Weber et al. 2008; McQuinn et al. 2015).

Given BST1047's dissimilarity to the faint, diffuse star-forming satellites of the Local Group, another comparison would be to larger LSB galaxies. BST1047's extremely low surface brightness is similar to the ultra-diffuse galaxies (UDGs) known to populate group and cluster environments, but these UDGs are typically red with little evidence for recent star formation (Koda et al. 2015; van Dokkum et al. 2015; Lee et al. 2017), making them a poor match to BST1047. Instead, blue gas-rich field LSBs may make a better comparison sample. BST1047 shares many of the properties of field LSBs, but taken to extremes. For example, the most diffuse LSB in the "(Almost) Dark" sample is Coma P, with peak surface brightness $\mu_B \approx 26.6\ {\rm mag\ arcsec^{-2}}$, $B - V = 0.13$, and gas fraction $f_g = 0.97$ (Janowiecki et al. 2015; Ball et al. 2018). BST1047 is similar in optical size and color to Coma P, but an order of magnitude lower in luminosity density. And while the total gas mass of both systems is comparable, BST1047's peak H I column of $\sim 1\ M_\odot\ {\rm pc^{-2}}$ makes it lower by a factor of four compared to Coma P.

Field LSBs are also marked by stochastic and inefficient star formation histories (Schombert & McGaugh 2014, 2015), likely due to their low gas densities, often below that thought necessary to trigger widespread star formation (e.g., van der Hulst et al. 1993; McGaugh & de Blok 1997; Wyder et al. 2009). Such an SFR must also be true for BST1047, given the need for a rapidly declining SFR to explain the optical/UV colors, stellar mass, and FUV and Hα star formation tracers discussed previously. While the gas densities in BST1047 are likely too low to sustain star formation, a

recent, short-lived, and now-declining burst of star formation could have been triggered by a tidal encounter in the Leo I group. BST1047's association with the Leo Ring's southern H I spur, along with the object's own H I tidal tails, are consistent with such a scenario, possibly involving the nearby spiral M96.

In this scenario, then, BST1047 would simply represent the most diffuse tail of the field LSB galaxy population, involved in an interaction in the group environment. If so, the object should follow the well-established baryonic Tully–Fisher (BTF) relationship (McGaugh et al. 2000; McGaugh 2011). Given its baryonic mass of $6 \times 10^7 M_\odot$, the BTF of McGaugh (2011) predicts a velocity width of of $\Delta v \approx 2 \times v_c = 67\,\mathrm{km\,s^{-1}}$. This is significantly larger than the observed $16\,\mathrm{km\,s^{-1}}$ H I velocity gradient, but could be accommodated if the galaxy is observed largely face on, with an inclination of roughly 15°. Unfortunately, while the imaging in Figure 2 does not suggest a highly inclined geometry, BST1047's extremely diffuse nature and irregular morphology makes inclination estimates difficult.

Discriminating between these various scenarios to explain BST1047 will require additional data. Of particular use would be detailed 21 cm mapping of the system, to resolve whether the velocity gradient is a sign of rotational motion or tidal shear. Similarly, deep imaging of BST1047 by the *Hubble Space Telescope* or the *James Webb Space Telescope* would yield information on the age and metallicity of BST1047's stellar populations—detecting an old red giant branch would provide strong argument against the tidal dwarf scenario. With such extreme properties compared to known extragalactic objects, BST1047 will provide important constraints on processes driving the formation, evolution, and destruction of diffuse galaxies in group environments.

We thank Stacy McGaugh and the referee for many helpful suggestions. This work was supported in part through NSF grant 1108964 to J.C.M. The Westerbork Synthesis Radio Telescope is operated by the ASTRON (Netherlands Institute for Radio Astronomy) with support from the Netherlands Foundation for Scientific Research (NWO).

Facilities: CWRU:Schmidt, WSRT.

ORCID iDs

J. Christopher Mihos https://orcid.org/0000-0002-7089-8616
Paul Harding https://orcid.org/0000-0003-3442-6248

References

Amorisco, N. C., & Loeb, A. 2016, MNRAS, 459, L51
Ball, C., Cannon, J. M., Leisman, L., et al. 2018, AJ, 155, 65
Bell, E. F., & de Jong, R. S. 2001, ApJ, 550, 212
Bigiel, F., Leroy, A., Walter, F., et al. 2008, AJ, 136, 2846
Bigiel, F., Leroy, A., Walter, F., et al. 2010, AJ, 140, 1194
Bournaud, F., Duc, P.-A., Amram, P., Combes, F., & Gach, J.-L. 2004, A&A, 425, 813
Bruzual, G., & Charlot, S. 2003, MNRAS, 344, 1000
Caldwell, N. 2006, ApJ, 651, 822
Cannon, J. M., Martinkus, C. P., Leisman, L., et al. 2015, AJ, 149, 72
Clark, P. C., & Glover, S. C. O. 2014, MNRAS, 444, 2396
Dalcanton, J. J., Spergel, D. N., & Summers, F. J. 1997, ApJ, 482, 659
Donahue, M., Aldering, G., & Stocke, J. T. 1995, ApJL, 450, L45
Draine, B. T. 2003, ApJ, 598, 1017
Duc, P.-A., Brinks, E., Springel, V., et al. 2000, AJ, 120, 1238
Graham, J. A., Phelps, R. L., Freedman, W. L., et al. 1997, ApJ, 477, 535
Haan, S., Schinnerer, E., Emsellem, E., et al. 2009, ApJ, 692, 1623
Hoffman, G. L., Lu, N. Y., Salpeter, E. E., & Connell, B. M. 1999, AJ, 117, 811
Hunter, D. A., Elmegreen, B. G., & Ludka, B. C. 2010, AJ, 139, 447
Impey, C., Bothun, G., & Malin, D. 1988, ApJ, 330, 634
Irwin, M. J., Belokurov, V., Evans, N. W., et al. 2007, ApJL, 656, L13
Jang, I. S., & Lee, M. G. 2017, ApJ, 836, 74
Janowiecki, S., Leisman, L., Józsa, G., et al. 2015, ApJ, 801, 96
Kennicutt, R. C., & Evans, N. J. 2012, ARA&A, 50, 531
Koda, J., Yagi, M., Yamanoi, H., & Komiyama, Y. 2015, ApJL, 807, L2
Krumholz, M. R., McKee, C. F., & Tumlinson, J. 2009, ApJ, 699, 850
Lee, M. G., Kang, J., Lee, J. H., & Jang, I. S. 2017, ApJ, 844, 157
Leisman, L., Haynes, M. P., Janowiecki, S., et al. 2017, ApJ, 842, 133
Leitherer, C., Schaerer, D., Goldader, J. D., et al. 1999, ApJS, 123, 3
Lelli, F., Duc, P.-A., Brinks, E., et al. 2015, A&A, 584, A113
McGaugh, S. S. 2011, PhRvL, 106, 121303
McGaugh, S. S., & Bothun, G. D. 1994, AJ, 107, 530
McGaugh, S. S., & de Blok, W. J. G. 1997, ApJ, 481, 689
McGaugh, S. S., Schombert, J. M., Bothun, G. D., & de Blok, W. J. G. 2000, ApJL, 533, L99
McQuinn, K. B. W., Skillman, E. D., Berg, D., et al. 2013, AJ, 146, 145
McQuinn, K. B. W., Skillman, E. D., Dolphin, A., et al. 2015, ApJ, 812, 158
Meisner, A. M., & Finkbeiner, D. P. 2014, ApJ, 781, 5
Michel-Dansac, L., Duc, P.-A., Bournaud, F., et al. 2010, ApJL, 717, L143
Miville-Deschênes,, M.-A., & Lagache, G. 2005, ApJS, 157, 302
Mihos, J. C., Durrell, P. R., Ferrarese, L., et al. 2015, ApJL, 809, L21
Mihos, J. C., Harding, P., Feldmeier, J. J., et al. 2017, ApJ, 834, 16
Mo, H. J., Mao, S., & White, S. D. M. 1998, MNRAS, 295, 319
Murphy, E. J., Condon, J. J., Schinnerer, E., et al. 2011, ApJ, 737, 67
Oosterloo, T., Morganti, R., Crocker, A., et al. 2010, MNRAS, 409, 500
Ryan-Weber, E. V., Begum, A., Oosterloo, T., et al. 2008, MNRAS, 384, 535
Sandage, A., & Binggeli, B. 1984, AJ, 89, 919
Schlafly, E. F., & Finkbeiner, D. P. 2011, ApJ, 737, 103
Schneider, S. 1985, ApJL, 288, L33
Schneider, S. E., Salpeter, E. E., & Terzian, Y. 1986, AJ, 91, 13
Schneider, S. E., Skrutskie, M. F., Hacking, P. B., et al. 1989, AJ, 97, 666
Schombert, J., & McGaugh, S. 2014, PASA, 31, e036
Schombert, J., & McGaugh, S. 2015, AJ, 150, 72
Schombert, J., McGaugh, S., & Maciel, T. 2013, AJ, 146, 41
Schombert, J. M., McGaugh, S. S., & Eder, J. A. 2001, AJ, 121, 2420
Thilker, D. A., Donovan, J., Schiminovich, D., et al. 2009, Natur, 457, 990
van der Hulst, J. M., Skillman, E. D., Smith, T. R., et al. 1993, AJ, 106, 548
van Dokkum, P. G., Abraham, R., Merritt, A., et al. 2015, ApJL, 798, L45
van Zee, L., Haynes, M. P., Salzer, J. J., & Broeils, A. H. 1997, AJ, 113, 1618
Wakker, B. P., & van Woerden, H. 1997, ARA&A, 35, 217
Watkins, A. E., Mihos, J. C., Harding, P., & Feldmeier, J. J. 2014, ApJ, 791, 38
Weilbacher, P. M., Duc, P.-A., Fritze v. Alvensleben, U., Martin, P., & Fricke, K. J. 2000, A&A, 358, 819
Wyder, T. K., Martin, D. C., Barlow, T. A., et al. 2009, ApJ, 696, 1834